Silicon-coated gold nanodiffraction grating structures as plasmonic absorbers for short-wavelength infrared light

Tsubota, Tatsuya ; Arai, Naoyuki ; Harada, Atsuya ; Uesugi, Akio ; Sugano, Koji ; Isono, Yoshitada

(Citation)
Journal of the Optical Society of America B,38(10):2863-2872

(Issue Date)
2021-10-01

(Resource Type)
journal article

(Version)
Accepted Manuscript

Silicon-coated gold nano diffraction grating structures as plasmonic absorber for short wavelength infrared light

TATSUYA TSUBOTA,[1] NAOYUKI ARAI,[1] ATSUYA HARADA,[1] AKIO UESUGI,[1] KOJI SUGANO,[1,*] AND YOSHITADA ISONO[1,]

[1]*Department of Mechanical Engineering, Graduate School of Engineering, Kobe University, Kobe, Hyogo 657-8501, Japan*
**sugano@mech.kobe-u.ac.jp*

Abstract: As a plasmonic absorber for short-wavelength infrared hyperspectral imaging, a silicon-coated gold nano diffraction grating structure is proposed. This plasmonic absorber leads to absorption peaks in short-wavelength infrared region by high refractive index of silicon coating on gold grating. It is relatively easy to be fabricated with smaller size than those of already known absorbers. By performing fabrication, simulation, and measurement, we demonstrate the sharp absorption peaks of short-wavelength infrared light using only 400−1000 nm grating interval. We believe this miniaturized absorber will enable to be applied to hyperspectral imaging without a spectroscope owing to its sharp absorption peak at a specific wavelength.

1. Introduction

In recent years, demand for non-destructive and non-contact inspections using short-wavelength infrared (SWIR, wavelength range: 1–3 μm) spectroscopy has increased. SWIR light is highly transparent to substances such as package films and liquids, as well as unique absorption characteristics to water. Water absorbs only specific wavelength light (1450–1500 nm) in contrast to other wavelengths. Therefore, changes in the amount of water generated due to spoilage inside food can be detected easily. SWIR spectroscopy is used in various applications, such as medicine inspections [1], medical diagnoses [2, 3], and food inspections [4-7]. However, the currently marketed SWIR detectors require optical equipment such as a diffraction grating spectroscope for hyperspectral imaging [8, 9]. The additional equipment results in high cost and large device size, as well as considerable detection noise due to radiant heat from optical components [10]. Therefore, absorbers with wavelength dependence in the SWIR wavelength range of detectors are expected to enable hyperspectral imaging without requiring diffraction grating spectroscopy. By integrating the structures of SWIR detectors and absorbers with various absorption peak wavelengths as one imaging pixel, various wavelength bands can be detected instantly without using the conventional diffraction grating spectroscope. Various studies regarding wavelength-dependent plasmonic absorbers have been reported [11, 12], where metal nanostructures such as nanorods [13, 14], nanofins [15-17], metal-insulator-metal (MIM) [18] and grating structures [19-21] for bio-chemical or microelectromechanical system (MEMS) optical sensors [21-25] have been reported. However, a full width at half maximum (FWHM) of the structures proposed in Ref. [14] is about 170 nm. Therefore, it is challenging to obtain a narrow-band absorption peak using nanorods. Nanofins are challenging to fabricate because of their high-aspect-ratio nanostructures, which result in low structural controllability. Because MIM structures control the absorption wavelength based on the thickness of the insulator thin film, it is difficult to fabricate multiple absorbers with different film thicknesses on a same substrate to yield different absorption peak wavelengths for sensor applications. Grating structures have been used as spectroscopic elements because they can

yield a narrow band absorption peak and good controllability for absorption peak wavelengths by changing the grating interval. The interval required for SWIR absorption is similar to the wavelength, as described in Section 2. Thus, absorber miniaturization for high-spatial-resolution hyperspectral imaging is restricted. Hence, we focus on miniaturized SWIR absorbers with a narrow band absorption peak with a FWHM of less than 100 nm in the wavelength ranged from 1000 to 2000 nm (generally used for food inspection), excellent controllability, and a wide control wavelength range on the same substrate.

Herein, we propose silicon (Si)-coated gold (Au) nano diffraction grating structures, which are relatively easy to fabricate because of the excellent compatibility of these materials in nano/microscale MEMS fabrication. The optical characteristics of grating structures are significantly affected by a refractive index (dielectric index) of the surroundings. Therefore, by coating the grating structures with Si, it is expected to reduce the grating interval, thereby resulting in a high refractive index and an excellent integration with MEMS.

In this study, we fabricated, simulated, and measured Si-coated Au nano diffraction grating structures. The effects of the Si coating thickness and the height, grating interval, and width of the Au nano diffraction grating structures on the optical characteristics are reported herein.

2. Principle of NIR absorption

Propagating electromagnetic waves combine with the collective vibration of free electrons at the interface between a metal and dielectric under certain conditions in the resonance state [26-29]. This phenomenon is known as surface plasmon polariton (SPP), and its behavior can be derived from Maxwell's equations. In this phenomenon, surface plasmon wave (SPW) propagates along the interface between the dielectric and metal. The SPW wavenumber (k_{sp}) is expressed as follows:

$$k_{sp} = \pm \frac{2\pi}{\lambda} Re\left(\sqrt{\frac{\varepsilon_s \varepsilon_m}{\varepsilon_s + \varepsilon_m}}\right), \quad (1)$$

where λ, ε_s, and ε_m denote the wavelength of light in vacuum, permittivity of dielectric, and complex permittivity of the metal, respectively.

The horizontal component of the diffracted light at an incidence angle θ (k_x) is expressed as follows:

$$k_x = \frac{2\pi}{\lambda}\sqrt{\varepsilon_s}\sin\theta + \frac{2m\pi}{d}, \quad (2)$$

where m and d denote the diffraction mode with a positive or negative integer and a grating interval, respectively. SPP is generated when k_{sp} and k_x match, and SPP can be observed at the wavelength intersecting k_{sp} and k_x. To satisfy the resonance condition, a metal whose real part of the refractive index is negative must be used. Gold, silver, and aluminum are typically used in wavelength regions of visible light and longer [30]. We used Au because it is highly compatible with MEMS and less likely to cause surface oxidation.

When we consider a simple case in which light is incident on an Au plane, k_x contains no second term. Consequently, no intersections exist and hence no SPP generation. Although a method using a prism as a medium is easy and often used to match k_{sp} and k_x, it prevents the miniaturization of sensors. Therefore, absorbers with metal diffraction grating structures were used in this study. The resonance wavenumber (or wavelength) and the electromagnetic intensity are affected by d and θ. As an example, their relationships when using Au diffraction gratings with $d =$ 600 nm and $d =$ 2000 nm are shown in Figs. 1(a) and (b), respectively. x and y axes mean the wavenumber and the wavelength of k_{sp} and k_x, respectively. In this study, the target wavelength ranged from 1000 to 2000 nm. The angle of incidence was fixed at $\theta =$ 30° because of the specifications of the measuring equipment used in this study, as described

in Section 3. In the case of $d =$ 600 nm, as shown in Fig. 1(a), no intersections were observed in the target wavelength range. By contrast, in the case of $d =$ 2000 nm, as shown in Fig. 1(b), intersections were observed at wavelengths of 1506, 1021, and 1007 nm. Therefore, by selecting the appropriate d and θ, SPP is generated by simply injecting light without an additional optical system, such as a prism, because of the intersection. In this regard, several studies pertaining to the control of the absorption wavelength by changing d or θ have been reported [31, 32].

However, because a sufficient number of diffraction gratings is required to generate SPPs, it is difficult to reduce the size of an absorber with $d =$ 2000 nm. Therefore, we propose Si-coated Au nano diffraction grating structures. The relationship between k_{sp} and k_x at $d =$ 600 nm is shown in Fig. 1(c). We can confirm that intersection wavelengths of 1628, 1263, and 1146 nm were observed; in other words, SPP is generated in the SWIR region. In the cases shown in Figs. 1(a) and (b), the SPW propagates at the interface between vacuum (or atmosphere) and Au. By coating Si (which has a dielectric constant of 11.8–12.8 and a refractive index of 3.44–3.58 in the SWIR region) on the Au diffraction gratings, the SPW propagates between Au and Si, and the absorption wavelength can be controlled. Therefore, we assume that SPPs can be generated in the SWIR region even at a smaller grating interval of approximately 30% or less owing to the refractive index of Si. This is expected to contribute to the further miniaturization of SWIR sensors.

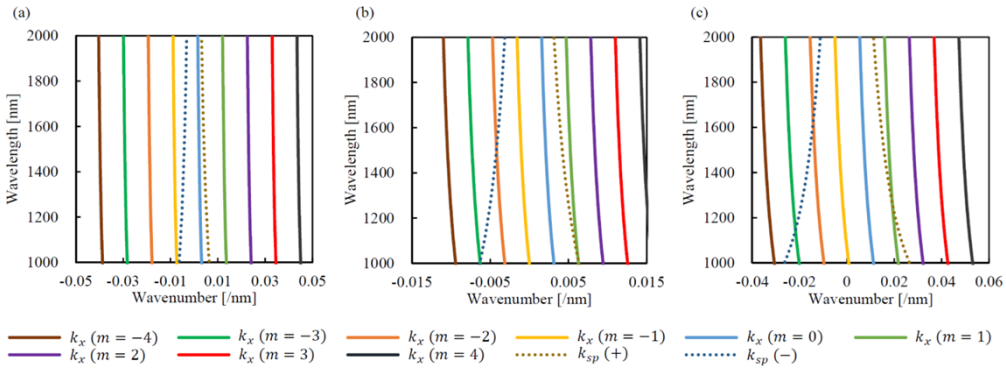

Fig. 1. Calculated relationship between resonance wavelength and wavenumber of SPW wavenumber k_{sp} and horizontal component of diffracted light k_x at wavelength ranging from 1000 to 2000 nm. x and y axis mean the wavenumber and the wavelength of k_{sp} and k_x, respectively. Angle of incidence fixed at $\theta =$ 30°. Relationship when using Au diffraction gratings with (a) $d =$ 600 nm, (b) $d =$ 2000 nm (both without Si coating), and (c) $d =$ 600 nm (with Si coating).

3. Methods

3.1 Structure

Figure 2 shows a schematic image and parameters of the Si-coated Au nano diffraction grating structures. The cross-sectional structures of the Au gratings and the coated Si depend on the fabrication process. We carried out the preliminary fabrication experiments to obtain the resulting structure and the available structural dimensions. In Section 3.1, the fabrication process, the fabrication result, and the parameters for simulations and experiments were presented.

For the diffraction grating structures, line and space patterns with length of 20 μm were fabricated on a Au thin film. First, a 10-nm-thick Cr thin film and a 100-nm-thick Au thin film were sequentially deposited on a bulk Si wafer using electron beam (EB) vapor deposition

equipment. Next, diluted positive resist ZEP 520A (Nippon Zeon) was spin coated onto the Au layer for EB lithography, followed by pre-baking on a hot plate. Subsequently, EB lithography of the Au nano diffraction grating patterns was performed. Subsequently, Au vacuum deposition and subsequent lift-off were performed to fabricate the Au nano diffraction gratings. Finally, Si was deposited via sputtering.

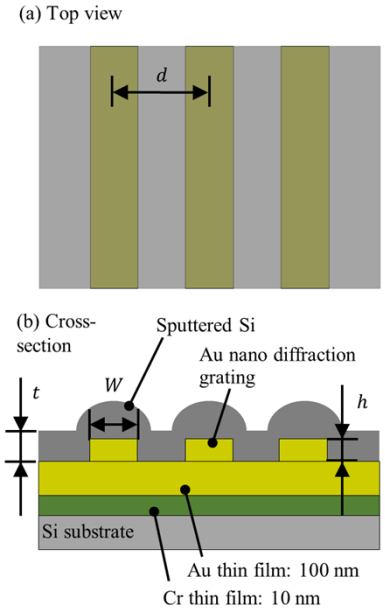

Fig. 2. Schematic illustration and parameters of Si-coated Au nano diffraction grating structures. Au line and space patterns with 20 μm length are fabricated on Au thin film and then Si is deposited.

Figure 3 shows scanning electron microscopy (SEM) images of the fabricated Si-coated Au nano diffraction grating structures. Figures 3(a) and (b) show the Au nano diffraction gratings before they were coated with Si. Figures 3(c) and (d) show the cross-sectional images. The cross-sectional shape of the nano diffraction gratings was trapezoidal. The coating Si was complicated structure that covered the nano diffraction gratings and contained dents. The measured average values of the Si coating thickness (t), grating height (h), grating interval (d), and grating width (W) of the Si-coated Au nano diffraction grating structures are shown in Table 1. t was controlled by sputtering time for absorption peaks in the SWIR region. These were determined as a parameter for simulations and experiments.

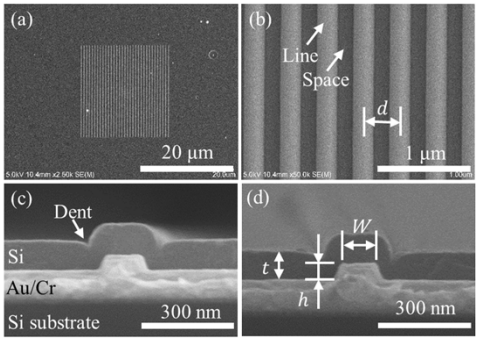

Fig. 3. SEM images of fabricated Si-coated Au nano diffraction grating structures, which are fabricated on Au thin film via EB lithography, Au vapor deposition, and Si sputtering. (a), (b) show top view of Au nano diffraction gratings prior to coating Si. (c), (d) show cross-sectional images of Au nano diffraction gratings after coating Si.

Table 1. Average values of measured grating height (h), thickness of Si coating (t), grating interval (d), and grating width (W) of Au nano diffraction grating structures

Dimension parameters	Design [nm]
Grating height (h)	40
Si coating thickness (t) (Sputtering time [min])	0, 77, 93, 102, 119 (0, 12.5, 15.0, 17.5, 20.0)
Grating interval (d)	400, 500, 600, 700, 800, 900, 1000
Grating width (W)	23, 45, 69, 101, 121, 141, 170, 202

3.2 Modeling

As a finite differential time domain (FDTD) method, we used FDTD Solutions (Lumerical), which is commercially available simulation software. The simulation model shown in Fig. 4 was designed based on the dimensions and shapes obtained from the SEM images. In measurement, angle of light θ through the reflective objective lens irradiating the absorber ranged from 16° to 45°. Therefore, we set $\theta =$ 30° because the median value had peak intensity. We applied the broadband fixed angle source technique (BFAST) to the light source, which is a plane wave and can calibrate different incident angles for each wavelength. The BFAST is effective when using an angled light source in a periodic structure. For the periodic boundary condition, we used the BFAST symmetric boundary condition to shorten the simulation time for the x- and y-planes. The perfectly matched layer absorption boundary condition was used for the z -plane. The width of the simulation area in the x-direction varied from 400 to 1000 nm, which corresponded to d. The length and height of the simulation area were set to 50 and 5400 nm, respectively, in the y- and z-directions. The data by Palik was used to set the complex refractive index of Au and Si as shown in Figs. 4(c)-(f). The mesh size of the complicated structures such as a dent or a corner was set to 3 nm. The mesh size was determined because no significant effect was confirmed at 3 nm or less. The auto-meshing function of the FDTD software was adapted to the other part. In the simulation, the absorption spectra of the Si-coated Au nano-diffraction grating structures were calculated. We investigated the effects of h, t, d, and W on the absorption spectrum and absorption peak wavelengths. The reflection and transmission spectra were calculated via FDTD simulation at wavelength of 1000–2000 nm, and the absorption was calculated as $A = 100 - T - R$. In addition, the electric field intensity distributions at the absorption peak wavelengths were evaluated.

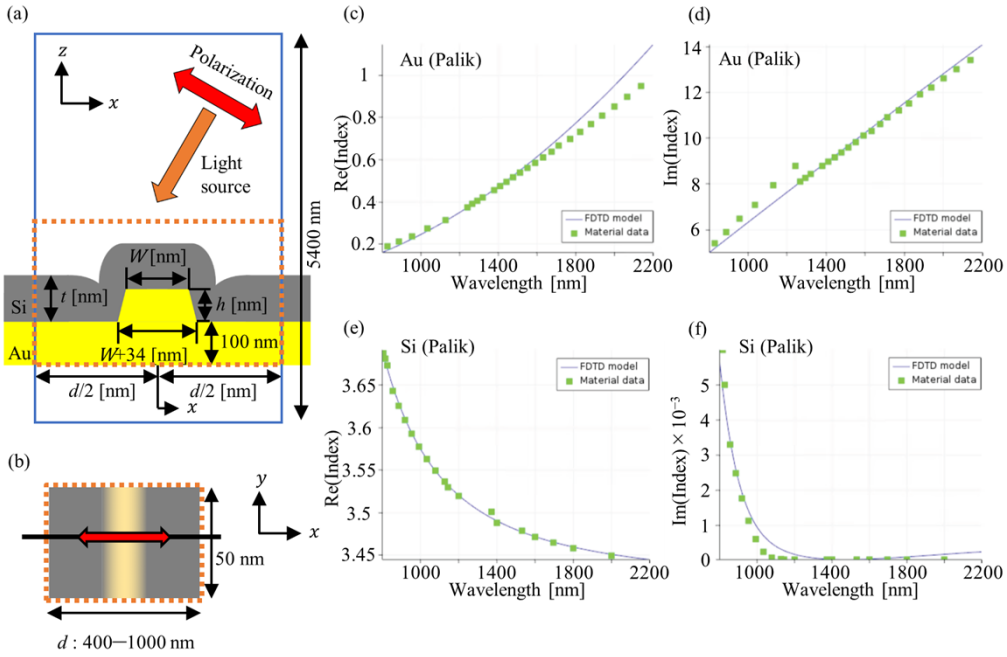

Fig. 4. Simulation model and complex refractive indices using FDTD Solutions (Lumerical); model is based on dimensions and shapes obtained from SEM image. Periodic boundary condition was used. (a) Sectional view. (b) Top view. (c)-(f) complex refractive indices of (c), (d) Au, and (e), (f) Si. Plots and solid lines indicate discrete material data and fitting result of refractive indices, respectively.

3.3 Measurement

Absorption A [%] is expressed in terms of transmittance T [%] and reflectance R [%] as follows: $A = 100 - T - R$. In this study, the absorption spectra were calculated as $A = 100 - R$ because the transmission of the Au thin film was negligible since the thickness of the Au layer was 100 nm, which provided a low transmittance of 2% or less calculated by the simulation. The reflectance was measured using an ultraviolet–visible/near-infrared microspectrophotometer (MSV-5200DGK, JASCO). A Cassegrain-type reflective objective lens equipped with a microspectrophotometer was used. A plane Au sample without patterns was used as a reference for the reflection spectra. The wavelength range for measurement was set from 1000 to 2000 nm.

4. Results

4.1 Effects of Si coating and grating height (h)

We investigated the effects of the grating height and Si coating using the FDTD simulation. Figure 5 shows the simulated absorption spectra at $t =$ 102 nm, $d =$ 600 nm, $W =$ 101 nm, and $h =$ 30–50 nm. At $h =$ 30 nm, we observed four absorption peaks at wavelengths of 1674, 1452, 1242, and 1170 nm, although no absorption peaks were observed without Si coating, as shown in Fig. 5(i). The spectrum without a Si coating ($t =$ 0 nm) shows the absorption of less than 4% without peaks. We found the Si coating contributed to the absorption of the SWIR light in simulation as mentioned in Sections 1 and 2. The above mentioned absorption peaks are referred to herein as the first, second, third, and fourth peaks, respectively. They are the ordinal numbers from longer wavelengths, and don't correspond to the diffraction mode shown

in Eq. (2) and Fig. 1. We discovered the absorption depended significantly on h. In particular, no second peak was observed when $h =$ 40−50 nm.

Figure 6 shows the electric field intensity distributions of each simulated absorption peak wavelength for $h =$ 30 nm. As shown in Figs. 6(c) and (d), the electric field at the corners of the trapezoidal upper base of the Au nano diffraction gratings are enhanced, and the electromagnetic waves propagate at the interface between Au and Si at wavelengths of 1242 nm (third) and 1170 nm (fourth). As shown in Figs. 6(a) and (b), the electric field strengthened in the dented part of the Si-coated gratings at wavelengths of 1674 nm (first) and 1452 nm (second). The first and second peaks indicated more significant effects by the dented part on the peak height than the third and fourth peaks. The lower absorption peaks were assumed to be due to the greater distance from the Au/Si interface to the dented part than to the Au corners, which resulted in a lower electric field (Fig. 6) and a greater absorption height. The dented part included significantly complicated structures, particularly in a narrow space.

Figure 7 shows the simulated and the experimentally measured absorption spectra of the absorbers with $d =$ 600 nm, $W =$ 101 nm, and $t =$ 102 nm or $t =$ 0 nm (without a Si coating). When $t =$ 0 nm, an absorption of 5% or less without peaks at wavelengths from 1000 to 2000 nm was observed, whereas the absorber with a Si coating of $t =$ 102 nm indicated large absorption peaks at wavelengths of 1591, 1412, 1165, and 1100 nm. We also confirmed the Si coating contributed to the absorption of the SWIR light in experiment. When $t =$ 0 nm, neither the simulated nor measured results indicated an absorption peak in the SWIR region. These results are consistent with theory because the case does not involve any intersections in the dispersion relation shown in Fig. 1(a). The second peak has a high absorption rate of 84.8% and a narrow bandwidth with a FWHM of 78 nm in the SWIR region. This is well below about 100 nm of the absorbers reported in recent study [19].

In this paragraph, the simulated and the experimental results were compared. No second peak was observed when $h =$ 40−50 nm, and the absorption (peak heights) of the simulated results for the first and second peaks were greatly different from those of the experimental results. The experimentally measured absorption at the wavelength of 1412 nm (second) was 84.8%, whereas that of 1452 nm (second) was 12.5% in the simulation for $h =$ 30 nm, which was significantly less than the measured value. Owing to the complicated structures such as dented part with narrow space, the accurate modeling for simulation is difficult; hence, the experimental and simulated results for the absorption height differ. In addition, we considered the complex refractive index of the sputtered Si differs from the Palik data used in this study because the sputtered Si is thought to be amorphous [33]. However, the simulated results exhibited the tendency of the experimental results for the peak wavelengths. The diffraction gratings with $h =$ 30 nm indicated four absorption peaks in simulation as well as the experimental results. We confirmed that the absorption peak wavelengths of the simulated results were similar to those of the experimental results, where it shifted to longer wavelength. Hence, we used a model with $h =$ 30 nm in the subsequent simulation to clarify the absorption peaks.

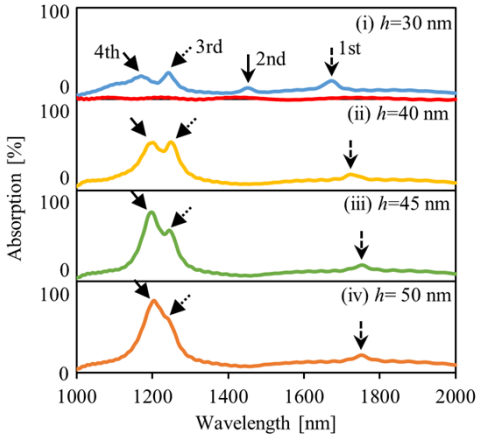

Fig. 5. Simulated absorption spectra of Si-coated Au nano diffraction grating absorbers with effect of height of nano diffraction gratings (h) for $t =$ 102 nm, $d =$ 600 nm, $W =$ 101 nm, and $h =$ 30−50 nm at wavelength ranging from 1000 to 2000 nm. In (i) $h =$ 30 nm, spectrum for $t =$ 102 nm (without a Si coating) is shown by red solid line.

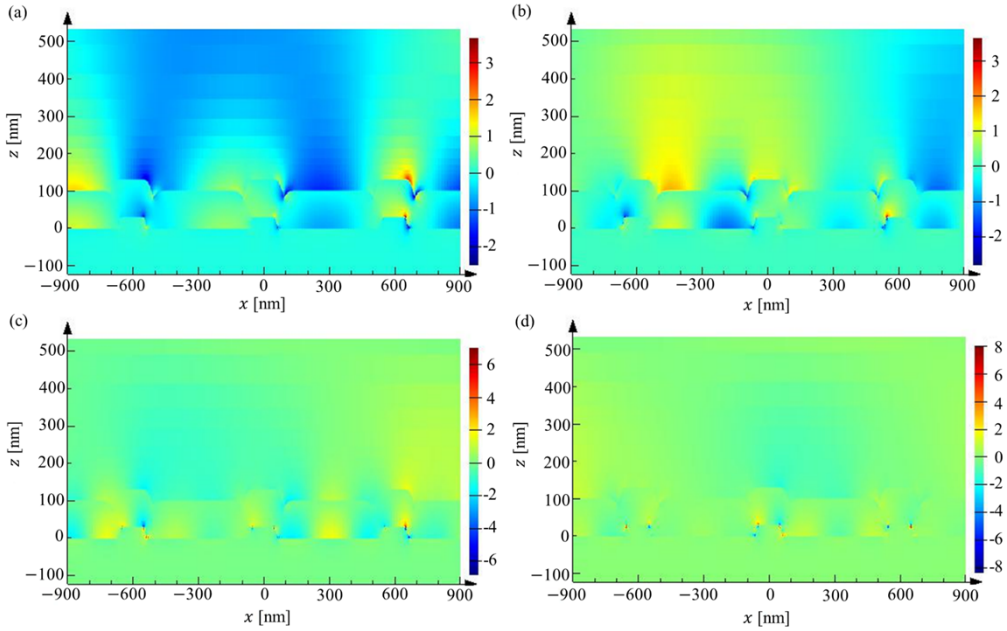

Fig. 6. Simulated electric field intensity distributions of each simulated absorption peak wavelengths of Si-coated Au nano diffraction grating absorbers for $t =$ 102 nm, $d =$ 600 nm, $W =$ 101 nm, and $h =$ 30 nm. (a) First peak at 1674 nm, (b) second peak at 1452 nm, (c) third peak at 1242 nm, and (d) fourth peak at 1170 nm.

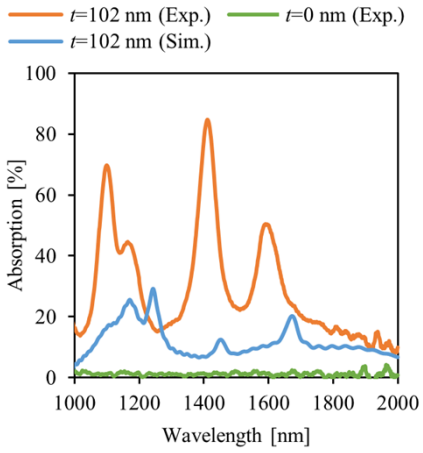

Fig. 7. Experimentally-measured (Exp.) and simulated (Sim.) absorption spectra of Si-coated Au nano diffraction grating absorbers for $d =$ 600 nm, $W =$ 101 nm, and $t =$ 102 nm at wavelength ranging from 1000 to 2000 nm. Case of $t =$ 0 nm (without a Si coating) is shown.

4.2 Effect of Si coating thickness (t)

Next, we investigated the effect of the Si coating thickness (t). Figures 8(a) and (b) show the simulated and experimentally-measured absorption spectra at $t =$ 0, 77, 93, 102, and 119 nm; $d =$ 600 nm; and $W =$ 101 nm, respectively. The absorption spectra for the case without Au nano diffraction gratings are also shown.

In simulation, it was confirmed that the absorbers without grating structures indicated a slight change in the absorption wavelength depending on the Si coating thickness as shown in Fig. 8 (dotted lines); however, a clear absorption peak was not observed. On the other hands, the absorbers with grating structures showed clear absorption peaks. We confirmed the absorption peaks in SWIR region of 1000-2000 nm at t ranging from 77 to 119 nm used in this study. We found the absorption peak wavelengths shifted to longer as t increased focusing on the first and second peaks because these peaks were clearly observed without peak's superposition. The dependency of Si coating thickness is observed because the electric field of SPW goes out of the Si thin layer, ranging from 77 to 119 nm, as shown in Fig. 6.

In measurement, when $t =$ 77 nm, peak wavelengths were observed at 1387 nm (first), 1239 nm (second), 1081 nm (third), and 1009 nm (fourth). The peak wavelengths at $t =$ 77 nm were shorter than those at $t =$ 93 nm. When $t =$ 119 nm, the absorption peaks appeared at 1694 nm (first), 1493 nm (second), 1196 nm (third), and 1123 nm (fourth). We found the four absorption peak wavelengths shifted to longer with increasing t as with the simulation. The wavelength of the second peak increased by 254 nm from 1239 to 1493 nm as t increased from 77 to 119 nm. The peak wavelengths can be controlled by changing t. The relationship between t and the absorption peak wavelengths is shown in Fig. 9. In both results, we confirmed the absorption peaks due to the Si coating, and the absorption peak wavelengths shifted to longer as t increased.

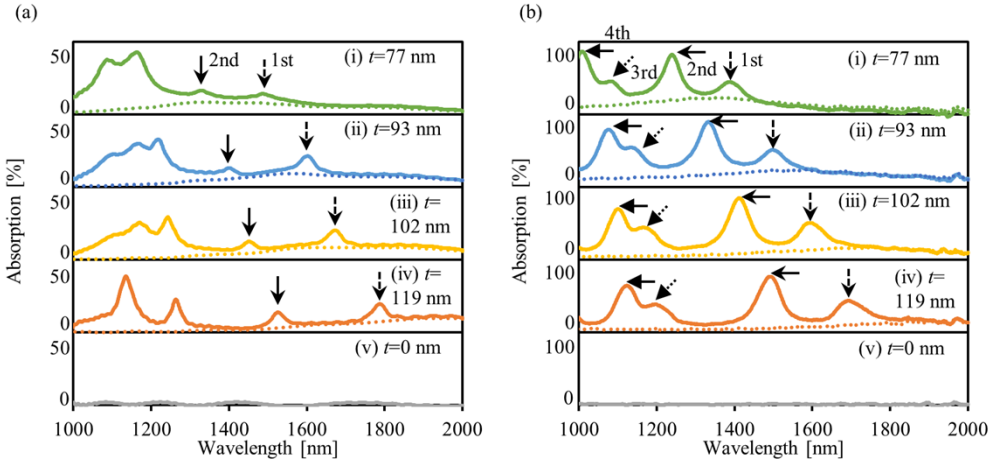

Fig. 8. Effect of Si coating thickness (t). (a) Simulated and (b) experimentally- measured spectra of Si-coated Au nano diffraction grating absorbers for $t =$ (i) 77, (ii) 93, (iii) 102, (iv) 119, (v) 0 nm ; $d =$ 600 nm; and $W =$ 101 nm at wavelength ranging from 1000 to 2000 nm. Solid and dotted lines indicate spectra in cases with and without Au nano diffraction gratings, respectively. Absorption ranges of these spectral graph in simulation and experiment are set from 0 to 50% and from 0 to 100%, respectively.

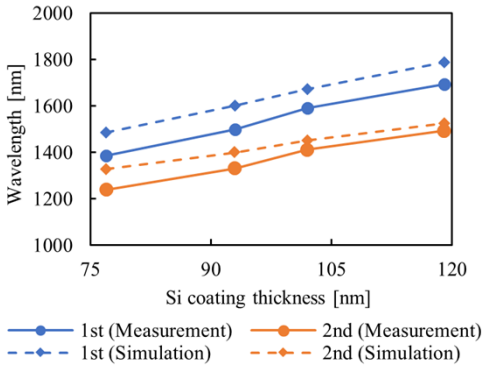

Fig. 9. Relationship between t and absorption peak wavelength ranging from 1000 to 2000 nm based on simulated and experimentally-measured results.

4.3 Effect of grating interval (d)

Next, we investigated the effect of the grating interval (d). Figures 10(a) and (b) show the simulated and experimentally-measured absorption spectra at $t =$ 102 nm, $d =$ 400–1000 nm, and $W =$ 101 nm, respectively. The absorption spectrum for the case without Au nano diffraction gratings are also shown in (viii).

In simulation, we found the absorption peak wavelengths shifted to longer as d increased focusing on the first and second peaks. This tendency is consistent with the theory as mentioned in Section 2. With increasing d from 400 to 1000 nm, the first and second peaks were shifted from 1463 to 1961 nm, and from 1238 to 1679 nm, respectively.

In measurement, when $d =$ 400 nm, the peak wavelengths appeared at 1370 nm (first), 1189 nm (second), and 1025 nm (third). Fourth and higher wavelength peaks were not observed. The fourth and fifth peaks with small absorption appeared at $d =$ 600 and 700 nm, respectively, when d increased. The peak wavelengths increased with d. When $d =$ 1000 nm,

the spectrum indicated absorption peaks at 1891 nm (first), 1693 nm (second), 1479 nm (third), and 1356 nm (fourth). At wavelengths shorter than the fourth peak, small absorption peaks appeared. The absorption peak wavelengths shifted to longer from 1189 to 1693 nm as d increased from 400 to 1000 nm, as indicated by the second peak, which demonstrated the highest absorption. The relationship between d and absorption peak wavelengths in simulation and experiment is shown in Fig. 11. From both results, we confirmed the absorption peak wavelengths shifted to longer as d increased, indicating good agreement between both results.

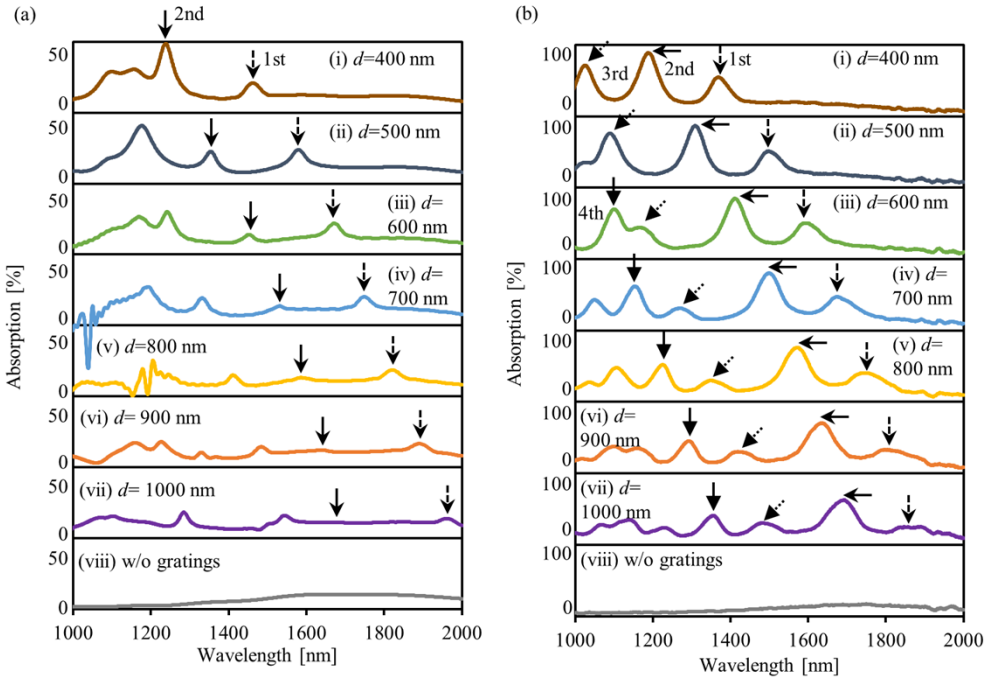

Fig. 10. Effect of grating interval (d). (a) Simulated and (b) experimentally-measured absorption spectra of Si-coated Au nano diffraction grating absorbers for $t =$ 102 nm, $d =$ 400–1000 nm ((i)–(vii)), and $W =$ 101 nm at wavelengths ranging from 1000 to 2000 nm. Case without Au nano diffraction gratings is shown (viii). Absorption ranges of these spectral graph in simulation and experiment are set from 0 to 50% and from 0 to 100%, respectively.

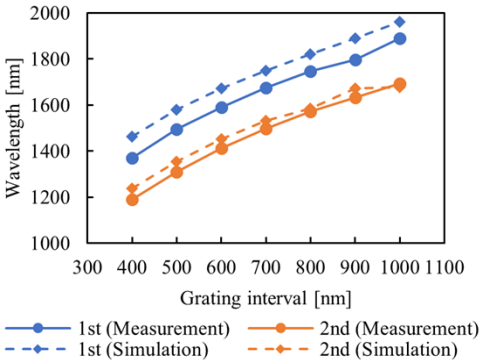

Fig. 11. Relationship between d and absorption peak wavelength ranging from 1000 to 2000 nm based on simulated and experimentally-measured results.

4.4 Effect of width of nano diffraction gratings (W)

Finally, we investigated the effect of the width of the nano diffraction gratings (W). Figures 12(a) and (b) show the simulated and experimentally-measured absorption spectra at $t =$ 102 nm, $d =$ 600 nm, and $W =$ 23−202 nm, respectively. In simulation, the wavelengths of the first and second peaks were independent of W ranging from 23 to 202 nm. This is because the width does not affect the peak wavelengths, according to the theory. In measurement, when $W =$ 45 nm, peak wavelengths were observed at 1610 nm (first), 1432 nm (second), 1200 nm (third), and 1060 nm (fourth). When $W =$ 170 nm, absorption peaks were observed at 1559 nm (first), 1438 nm (second), 1214 nm (third), and 1058 nm (fourth). The second peak wavelengths shifted slightly to longer wavelengths, and the first peak shifted to shorter wavelengths as W increased. The relationship between W and the absorption peak wavelengths in simulation and experiment is shown in Fig. 13. The tendency of experiment are consistent with the simulation.

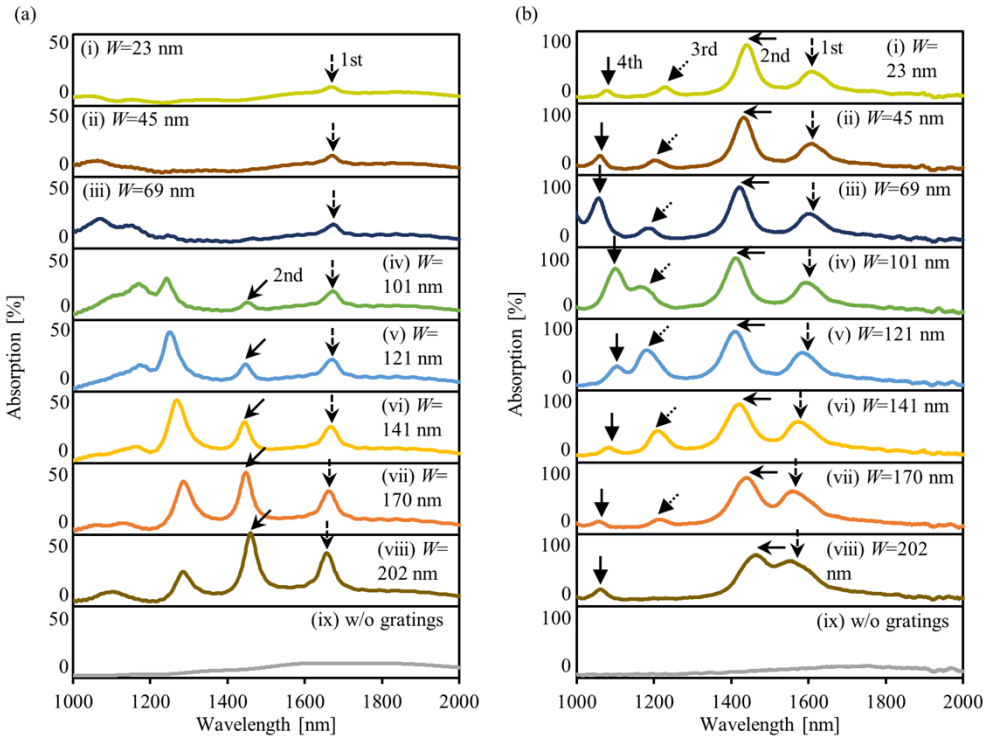

Fig. 12. Effect of width of nano diffraction gratings (W). (a) Simulated and (b) experimentally-measured absorption spectra of Si-coated Au nano diffraction grating absorbers with effect of W for $t =$ 102 nm, $d =$ 600 nm, and $W =$ 23−202 nm ((i)–(viii)) at wavelengths ranging from 1000 to 2000 nm. Case without Au nano diffraction gratings is shown in (ix). Absorption ranges of these spectral graph are set from 0 to 100% and from 0 to 50%, respectively.

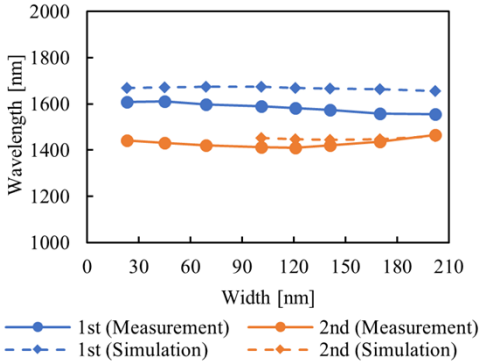

Fig. 13. Relationship between W and absorption peak wavelength ranging from 1000 to 2000 nm based on simulated and experimentally-measured results.

We discovered the effect of t or d prominent although that of W was less. By comparing between the simulated and experimentally-measured results, we confirmed that both indicated absorption peak wavelength shifts and hence validated the proposed structure. Furthermore, we demonstrated that coating the Au diffraction grating structures with Si reduced the grating interval. The grating interval of this proposed absorbers is 400-1000 nm for SWIR, which is much smaller than 1050-1350 nm of the absorbers reported in recent studies [19]. Therefore, we conclude that adopting the proposed absorber will result in the miniaturization of plasmonic optical sensors.

5. Conclusion

We herein propose Si-coated Au nano diffraction grating structures as miniaturized SWIR absorbers with a narrow band absorption peak, excellent controllability, and a wide control wavelength range on a same substrate. We performed nanofabrication, simulation using the FDTD method, and measurement for Si-coated Au nano diffraction grating structures. It was confirmed that Si coating contributed to the absorption of SWIR light at wavelength ranging from 1000 to 2000 nm owing to the high refractive index of Si. Three or four narrowband absorption peaks with a FWHM of approximately 75 nm were observed, and their maximum absorption was 86.6%. We found the absorption peak wavelengths shifted to longer as the Si coating thickness increased. Whereas the absorption peak wavelengths shifted to longer as the grating interval increased, a slight shift occurred owing to the grating width. We discovered that the grating interval and Si coating thickness effectively controlled the absorption peak wavelengths. Additionally, the required grating interval is 400-1000 nm, which is much smaller than those of the structures reported in recent studies. The experimental results exhibited the same tendency as the FDTD simulated results regarding the peak wavelengths. Therefore, we believe that this absorber will enable low-cost and miniaturized optical sensors leading to non-destructive and non-contact inspections without requiring a spectroscope.

Funding. KAKENHI Grant Number JP18H01847 and 19H02571, Japan Society for the Promotion of Science (501100001691)

Acknowledgments. This work was supported by Kyoto University Nano Technology Hub in "Nanotechnology Platform Project" sponsored by the Ministry of Education, Culture, Sports, Science and Technology (MEXT), Japan. This work was supported by Nanotechnology Platform of MEXT, Grant Number JPMXP09F20OS0013.

Disclosures. The authors declare no conflicts of interest.

Data availability. Data underlying the results presented in this paper are not publicly available at this time but may be obtained from the authors upon reasonable request.

References

1. M. Andre, "Multivariate analysis and classification of the chemical quality of 7-aminocephalosporanic acid using near-infrared reflectance spectroscopy," Anal. Chem. **75**, 3460-3467 (2003).
2. H. Koizumi, Y. Yamashita, A. Maki, T. Yamamoto, Y. Ito, H. Itagaki, and R. P. Kennan, "Higher-order brain function analysis by trans-cranial dynamic near-infrared spectroscopy imaging," J. Biomed. Opt. **4**, 403-413 (1999).
3. S. Luo, E. Zhang, Y. Su, T. Cheng, and C. Shi, "A review of NIR dyes in cancer targeting and imaging," Biomaterials **32**, 7127-7138 (2011).
4. D. Wu and D.-W. Sun, "Advanced applications of hyperspectral imaging technology for food quality and safety analysis and assessment: A review — Part II: Applications," Innov. Food Sci. Emerg. Technol. **19**, 15-28 (2013).
5. W.-H. Lee, M. S. Kim, H. Lee, S. R. Delwiche, H. Bae, D.-Y. Kim, and B.-K. Cho, "Hyperspectral near-infrared imaging for the detection of physical damages of pear," Journal of Food Engineering **130**, 1-7 (2014).
6. G. ElMasry, D.-W. Sun, and P. Allen, "Near-infrared hyperspectral imaging for predicting colour, pH and tenderness of fresh beef," Journal of Food Engineering **110**, 127-140 (2012).
7. Y. Jiang, C. Li, and F. Takeda, "Nondestructive detection and quantification of blueberry bruising using near-infrared (NIR) hyperspectral reflectance imaging," Sci. Rep. **6**, 1-14 (2016).
8. M. Manley, "Near-infrared spectroscopy and hyperspectral imaging: non-destructive analysis of biological materials," Chem. Soc. Rev. **43**, 8200-8214 (2014).
9. B. M. Nicolaï, K. Beullens, E. Bobelyn, A. Peirs, W. Saeys, K. I. Theron, and J. Lammertyn, "Nondestructive measurement of fruit and vegetable quality by means of NIR spectroscopy: A review," Postharvest. Biol. Technol. **46**, 99-118 (2007).
10. S. Ogawa, Y. Takagawa, and M. Kimata, "Broadband polarization-selective uncooled infrared sensors using tapered plasmonic micrograting absorbers," Sensors and Actuators A: Physical **269**, 563-568 (2018).
11. S. Ogawa, Y. Takagawa, and M. Kimata, "Elimination of Unwanted Modes in Wavelength-Selective Uncooled Infrared Sensors with Plasmonic Metamaterial Absorbers using a Subtraction Operation," Materials (Basel) **12**(2019).
12. S. Ogawa and M. Kimata, "Wavelength- or Polarization-Selective Thermal Infrared Detectors for Multi-Color or Polarimetric Imaging Using Plasmonics and Metamaterials," Materials (Basel) **10**(2017).
13. X. Huang, S. Neretina, and M. A. El-Sayed, "Gold nanorods: from synthesis and properties to biological and biomedical applications," Adv Mater **21**, 4880-4910 (2009).
14. A. V. Kabashin, P. Evans, S. Pastkovsky, W. Hendren, G. A. Wurtz, R. Atkinson, R. Pollard, V. A. Podolskiy, and A. V. Zayats, "Plasmonic nanorod metamaterials for biosensing," Nat Mater **8**, 867-871 (2009).
15. Y.-L. Ho, M. Abasaki, and J.-J. Delaunay, "Loop-Turn Optical Flows with Spectral Selectivity in Suspended Plasmonic Nanofin-Cavity Structure," ACS Photonics **2**, 730-737 (2015).
16. Y.-L. Ho, A. Portela, Y. Lee, E. Maeda, H. Tabata, and J.-J. Delaunay, "Hollow Plasmonic U-Cavities with High-Aspect-Ratio Nanofins Sustaining Strong Optical Vortices for Light Trapping and Sensing," Advanced Optical Materials **2**, 522-528 (2014).
17. E. Maeda, Y. Lee, Y. Kobayashi, A. Taino, M. Koizumi, S. Fujikawa, and J. J. Delaunay, "Sensitivity to refractive index of high-aspect-ratio nanofins with optical vortex," Nanotechnology **23**, 505502 (2012).
18. J. Hao, J. Wang, X. Liu, W. J. Padilla, L. Zhou, and M. Qiu, "High performance optical absorber based on a plasmonic metamaterial," Applied Physics Letters **96**(2010).
19. A. Sobhani, M. W. Knight, Y. Wang, B. Zheng, N. S. King, L. V. Brown, Z. Fang, P. Nordlander, and N. J. Halas, "Narrowband photodetection in the near-infrared with a plasmon-induced hot electron device," Nat. Commun. **4**, 1643 (2013).
20. S. Xiao, J. Zhang, L. Peng, C. Jeppesen, R. Malureanu, A. Kristensen, and N. A. Mortensen, "Nearly zero transmission through periodically modulated ultrathin metal films," Applied Physics Letters **97**(2010).
21. W. Chen, T. Kan, Y. Ajiki, K. Matsumoto, and I. Shimoyama, "NIR spectrometer using a Schottky photodetector enhanced by grating-based SPR," Opt. Express **24**, 25797-25804 (2016).
22. T. Tsubota, A. Uesugi, K. Sugano, and Y. Isono, "Wavelength-dependent near-infrared microbolometer for short-wavelength infrared light with gold nanowire grating optical absorber," Microsystem Technologies **27**, 997-1005 (2021).
23. K. Takegami, K. Nakafuji, N. Arai, A. Uesugi, K. Sugano, and Y. Isono, "Effect of clamped beam pattern on resonant frequency shift of microresonator under near-infrared laser irradiation," Jpn. J. Appl. Phys. **59**, SIII04 (2020).
24. K. Sugano, Y. Tanaka, A. Uesugi, E. Maeda, R. Kometani, and Y. Isono, "Detection of wavelength shift of near-infrared laser using mechanical microresonator-based sensor with Si-covered gold nanorods as optical absorber," Sensors and Actuators A: Physical **315**(2020).
25. E. Maeda and R. Kometani, "Sub-picometer multi-wavelength detector based on highly sensitive nanomechanical resonator," Applied Physics Letters **111**, 013102 (2017).

26. P. Zilio, D. Sammito, G. Zacco, and F. Romanato, "Absorption profile modulation by means of 1D digital plasmonic gratings," Opt. Express **18**, 19558-19565 (2010).
27. T. Iqbal and S. Afsheen, "Coupling efficiency of surface plasmon polaritons for 1D plasmonic gratings: role of under-and over-milling," Plasmonics **11**, 1247-1256 (2016).
28. F. Romanato, T. Ongarello, G. Zacco, D. Garoli, P. Zilio, and M. Massari, "Extraordinary optical transmission in one-dimensional gold gratings: near-and far-field analysis," Applied optics **50**, 4529-4534 (2011).
29. T. Ongarello, F. Romanato, P. Zilio, and M. Massari, "Polarization independence of extraordinary transmission trough 1D metallic gratings," Opt. Express **19**, 9426-9433 (2011).
30. P. B. Johnson and R. W. Christy, "Optical Constants of the Noble Metals," Physical Review B **6**, 4370-4379 (1972).
31. J. Dostálek and J. Homola, "Surface plasmon resonance sensor based on an array of diffraction gratings for highly parallelized observation of biomolecular interactions," Sensors and Actuators B: Chemical **129**, 303-310 (2008).
32. Z. Li, S. Butun, and K. Aydin, "Ultranarrow band absorbers based on surface lattice resonances in nanostructured metal surfaces," ACS nano **8**, 8242-8248 (2014).
33. M. V. Gorkunov, O. Y. Rogov, A. V. Kondratov, V. V. Artemov, R. V. Gainutdinov, and A. A. Ezhov, "Chiral visible light metasurface patterned in monocrystalline silicon by focused ion beam," Sci. Rep. **8**, 11623 (2018).